

Accessing quasi-flat f -bands to harvest large Berry curvature in NdGaSi

Anyesh Saraswati,¹ Jyotirmoy Sau,¹ Sudipta Chatterjee,¹ Sandip Kumar Kuila,² Bibhas Ghanta,^{3,4}
Anup Kumar Bera,^{3,4} Partha Pratim Jana,² Manoranjan Kumar,^{1,*} and Nitesh Kumar^{1,†}

¹*S. N. Bose National Centre for Basic Sciences, Salt Lake City, Kolkata-700106, India*

²*Department of Chemistry, Indian Institute of Technology, Kharagpur-721302, India*

³*Solid State Physics Division, Bhabha Atomic Research Centre, Mumbai-400085, India*

⁴*Homi Bhabha National Institute, Anushaktinagar, Mumbai-400094, India*

Bands away from the Fermi energy do not influence the electrical conduction. In typical rare-earth lanthanide compounds, the localized $4f$ -electrons have a weak effect on the electrical conduction, limiting their influence on the Berry curvature and, hence, the intrinsic anomalous Hall effect. However, a comprehensive study of the magnetic, thermodynamic, and transport properties of single-crystalline NdGaSi, guided by first-principles calculations, reveals a ferromagnetic ground state that induces a splitting of quasi-flat $4f$ electronic bands and positions them near the Fermi energy. The observation of an extraordinarily large intrinsic anomalous Hall conductivity of $1165 \Omega^{-1} \text{cm}^{-1}$ implies the direct involvement of localized states in the generation of non-trivial band crossings around the Fermi energy. These results are remarkable when compared to ferrimagnetic NdAlSi, which differs only in a non-magnetic atom (a change in the principal quantum number n of the outer p orbital) with the same number of valence electrons and does not exhibit any measurable anomalous Hall conductivity.

$4f$ -electrons are typically confined to the ion core and strongly shielded by the more delocalized $5d$ and $5p$ orbitals [1]. They, therefore, rarely contribute to electrical conduction, unlike their itinerant $3d$ -electron counterparts. Nevertheless, flat bands of $4f$ -electrons carry robust local magnetic moments and exhibit significantly enhanced spin-orbit coupling (SOC), which can theoretically generate large Berry curvatures (BC) via strong hybridization with dispersive bands and, hence, a substantial intrinsic anomalous Hall conductivity (AHC). However, the literature on the anomalous Hall effect (AHE) in rare-earth-based compounds is scarce, while the largest values have been reported in $3d$ -elements-based itinerant magnets. The dual role of conduction and magnetism by $3d$ -electrons ensures that SOC strongly modulates the electronic band structure, generating a substantial BC that deflects carriers transversely, leading to a large intrinsic contribution to the AHC [2–5]. On the other hand, in $4f$ -compounds, in general, the localized $4f$ -electrons only contribute to magnetism, while conduction is provided by more dispersive bands that don't constitute the f -electrons [6–9]. This decoupling dramatically reduces the amplitude of the BC in the conduction bands.

However, it has been argued that quasi-flat bands enhance the BC effects by effectively increasing the momentum-space separation between Weyl crossings resulting from time-reversal symmetry breaking [10–12]. In addition, if the quasi-flat bands coexist with dispersive bands just below the Fermi energy (E_F), the situation is prone to provide non-trivial crossing points, thereby enhancing the BC effect in the presence of SOC. To test this hypothesis, we have studied NdGaSi, which belongs to a large family of compounds with tetragonal symmetry [6, 13–25]. It has been shown that substitution in the Ga or Si site can drastically affect the magnetic exchange

mechanism, resulting in compounds exhibiting a variety of magnetic ground states such as ferrimagnetism (FIM), antiferromagnetism (AFM), helical states, and ferromagnetism (FM) [26]. We show that the magnetic ground state is closely related to the position of the quasi-flat f -bands, i.e., whether they form the valence band or remain unoccupied. In the case of NdGaSi, we show from magneto-transport, thermodynamic measurements, and first-principles calculations that the FM ground state ensures that the quasi-flat f -bands lie in the vicinity of E_F . This is further corroborated by the large enhancement of the density of states (DOS) at E_F and specific heat measurements resulting in an unusually large Sommerfeld coefficient. This ultimately leads to the observation of an extraordinarily large AHC due to the BC effect, in contrast to FIM NdAlSi, where the f -bands are pushed to the unoccupied states and therefore show vanishingly small AHC [13, 20].

We have successfully synthesized high-quality single crystals of NdGaSi, which crystallize in the tetragonal α -ThSi₂-type centrosymmetric structure (space group $I4_1/amd$). Both the single-crystal x-ray diffraction and neutron diffraction studies confirm that the non-rare-earth sites are equally occupied by Ga and Si, forming well-ordered repeating stacks of Nd and Ga/Si. The consecutive Nd-layers are separated by a distance of 3.57 Å, creating a distinctive layered arrangement (Fig. 1a). The detailed methodology for crystal growth, characterization, and structure determination is provided in Sec. IA of the supplementary information (SI) [27].

The field-cooled susceptibility $\chi(T)$ measurements (Fig. 1b) reveal a pronounced anisotropy, with the easy-axis susceptibility along the [001] direction being nearly two orders of magnitude higher than that along the [100] direction. This striking difference underscores the pres-

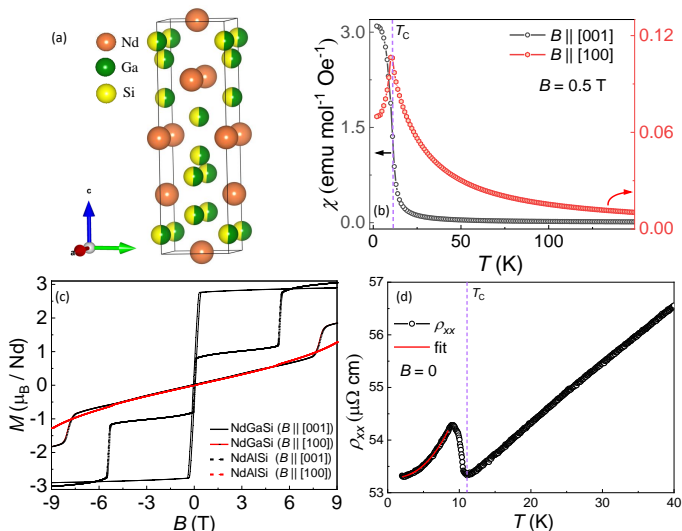


FIG. 1. (a) A tetragonal unit cell of NdGaSi. A simultaneous occupancy of Ga and Si sites (complete site mixing) imparts a centrosymmetric space group $I4_1/amd$. (b) Magnetic susceptibility (χ) measured under the field-cooled (FC) condition by applying the magnetic field along the in plane and out of the plane applied magnetic field. (c) Isothermal magnetization curves of NdAlSi and NdGaSi at 2 K with the magnetic field applied along [001] and [100]. (d) Longitudinal resistivity (ρ_{xx}) as a function of temperature under zero magnetic field, along with a fit (red) at low temperature to obtain the coefficient of electron scattering.

ence of strong magneto-crystalline anisotropy in the system, which is a common feature of other compounds in this series [6, 17, 20]. A clear anomaly at around $T_C = 11$ K for both directions confirms the onset of magnetic ordering. The out-of-plane susceptibility shows a sudden rise in magnetization with decreasing temperature, reminiscent of an FM. In contrast, the in-plane susceptibility reveals a cusp-like feature, with a peak at T_C , most likely arising from a weak AFM in the ab -plane due to a small spin canting away from the c -axis. Such non-colinearity typically arises in centrosymmetric systems due to SOC [28].

FM in NdGaSi is further indicated by a sharp and spontaneous saturation of magnetization to a value of $2.9 \mu_B/\text{Nd}$ when the magnetic field is applied along [001] in an isothermal magnetization measurement at 2 K. The corresponding magnetization along [100] increases monotonically with increasing magnetic field up to 9 T, except at 7.9 T, where a metamagnetic transition occurs. The magnetic behavior in NdGaSi is quite different from its sister compound NdAlSi, which chemically differs only in the nonmagnetic Ga/Al site occupancy. NdAlSi is known to exhibit FIM nature with a spontaneous magnetization of $1 \mu_B/\text{Nd}$ when the magnetic field is applied along c -axis. The full polarization of the Nd-moment, i.e., $3 \mu_B/\text{Nd}$, is only achieved after a magnetic field-induced meta-magnetic transition at 5 T (Fig. 1c).

NdGaSi exhibits metallic behavior down to 2 K (Fig. 1d), with a notable anomaly around 11 K in the longitudinal resistivity ρ_{xx} , consistent with the magnetic transition. The low-temperature curve below the magnetic ordering is best expressed by the Landau Fermi liquid behavior (2nd term) along with a gapped magnon contribution (3rd term) as $\rho_{xx} = \rho_0 + AT^2 + CT^2 e^{-\Delta/T}$, where ρ_0 represents the scattering of electrons from lattice imperfections [29–31]. We obtain $A = 0.624 \times 10^{-2} \mu\Omega \text{ cm K}^{-2}$ and $\Delta = 7.57$ K from the fit. NdGaSi exhibits a relatively small residual resistivity ratio (RRR) of ~ 1.66 , which could be the result of anti-site disorder between Si and Ga atoms. We will discuss the magnitude of A in the next section under the context of electron localization.

Analysis of low-temperature specific heat provides essential clues regarding localized states around E_F . NdGaSi exhibits a sharp λ -like peak around 11 K corresponding to the bulk magnetic transition (Fig. 2a). A broad hump centered around 15 K indicates the well-known Schottky anomaly which arises due to the splitting of the Nd^{3+} atomic levels induced by crystalline electric field (CEF) [32, 33]. The magnetic specific heat ($S_m(T) = \int \frac{C_m}{T} dT$) attains a value of $\sim R \ln 2$ below T_C (See inset of Fig. 2a), indicating the localized nature of $4f$ -electrons. Furthermore, the specific heat data below T_C can be expressed as $C_p(T) = \gamma T + \beta T^3 + \delta T^{3/2} e^{-\Delta/T}$, where the first, second, and third terms correspond to the electron, lattice, and magnon contributions, respectively [30, 33]. The dominant exponential behavior of $C_p(T)$ at a low temperature indicates the presence of a spin gap that arises due to anisotropic FM exchange, and fitting was carried out by fixing the lattice-related parameter obtained from that for LaGaSi in Sec. IV of SI [27], which gives a value of the magnon gap ($\Delta \sim 6.8$ K), consistent with that obtained from resistivity analysis. However, we find that the obtained Sommerfeld coefficient ($\gamma \sim 55.46 \text{ mJ mol}^{-1} \text{ K}^{-2}$) is relatively high compared to previously known Nd compounds [31, 34, 35] and strays away from typical itinerant systems. On the other hand, LaGaSi, which does not contain f -electrons, exhibits a reasonably small γ of $2.54 \text{ mJ mol}^{-1} \text{ K}^{-2}$. This suggests that the enhancement of DOS is mainly contributed by the f -electrons in NdGaSi.

The Sommerfeld coefficient (γ) dictates the distribution of the DOS around E_F . For a free electron model, $\gamma_{theo} = D(E_F) \pi^2 k_B^2 / 3$, where $D(E_F)$ is the DOS at E_F , and if we assume that all the DFT DOS comes from the free electron, then the theoretical value (γ_{theo}) is $\sim 43.39 \text{ mJ mol}^{-1} \text{ K}^{-2}$, significantly smaller than the experimentally observed value γ . The enhanced value of γ suggests the presence of correlated electrons at E_F [36, 37], which is consistent with the presence of f -states at E_F shown in Fig. 2c.

Our calculated spin-resolved DOS of NdGaSi unveils localized f -states at E_F . It reveals an FM ground state,

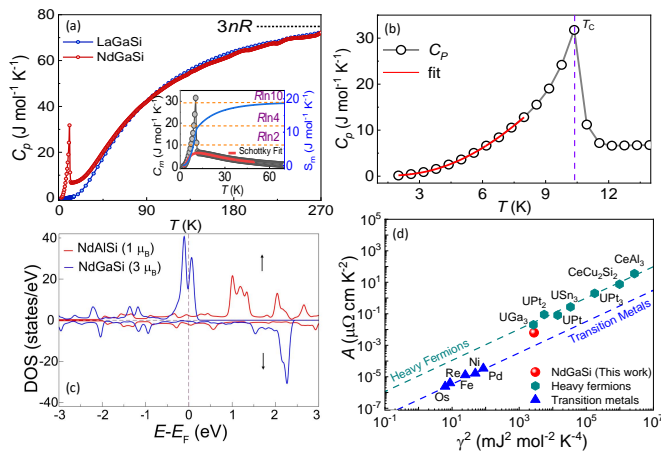


FIG. 2. (a) Specific heat of NdGaSi and NdAlSi as a function of temperature. The inset shows the variation of both magnetic specific heat and entropy as a function of temperature. (b) Specific heat data below 12 K with fitting. (c) Density of states of NdGaSi and NdAlSi in the ground state. (d) Kadowaki-Woods ratio of NdGaSi and its representation among itinerant and heavy Fermion systems.

where Nd 4*f*-electrons are the primary source of magnetism with a magnetic moment of 3 μ_B per formula unit. As illustrated in Fig. 2c (blue line), the spin-resolved DOS exhibits a tiny gap in the minority spin channel, while the majority spin channel remains metallic, indicating a nearly half-metallic behavior. In contrast, NdAlSi exhibits an FIM ground state with a low magnetic moment of 1 μ_B per formula unit, which can be understood in terms of the DOS, represented by a red curve in Fig. 2c. A small value of DOS at E_F corresponds to dispersive bands, which mostly comprise the Al and Si states (see Sec. VII of SI [27]). The large magnetic moment (3 μ_B) of NdGaSi can be achieved by depopulating the localized up-spin *f*-bands close to E_F that give rise to a significant peak in the DOS around the E_F (see blue curve in Fig. 2c). A significant peak in DOS arising from the localized up-spin *f*-electrons is also observed in EuAlSi [26], which exhibits an FM ground state.

The weaker hybridization strength of the 4*f*-4*p* (NdGaSi) compared to the 4*f*-3*p* (NdAlSi) along the *c*-axis plays a crucial role in magnetism [38, 39]. The super-exchange mechanism is highly favored in NdAlSi due to the strong 4*f*-3*p* hybridization, which discourages the formation of a local Nd moment and strongly favors a short-range super-exchange behavior, evident from spontaneous FIM behavior. NdGaSi, on the other hand, hosts a weaker 4*f*-4*p* hybridization than the former and strongly promotes a long-range 4*f*-4*f* Ruderman-Kittel-Kasuya-Yosida (RKKY) interaction, which results in a spontaneous FM behavior. This is highly favored by the majority of localized *f*-states around the E_F realized earlier, providing enough conducting states to support an

RKKY interaction [26].

To conclude our argument regarding the occupied localized states, we shift our focus to the Kadowaki-Woods ratio relating γ to the coefficient of the T^2 term in the longitudinal resistivity, A , i.e., $R_{KW} = A/\gamma^2$. This is used as a benchmark for electron localization, with a universal constant for heavy fermion systems ($R_{KW} \sim 10^{-5} \mu\Omega$ cm K² mol² mJ⁻²) and transition elements ($R_{KW} \sim 10^{-7} \mu\Omega$ cm K² mol² mJ⁻²) [40–42]. NdGaSi yields a value of $R_{KW} \sim 0.225 \times 10^{-5} \mu\Omega$ cm K² mol² mJ⁻², approximately two orders larger than itinerant systems but slightly smaller than conventional localized systems. This is depicted in Fig. 2d, where it lies in a regime best defined by moderately enhanced carrier localization but not to the extent of heavy-fermion systems.

The calculated electronic band structure of NdGaSi with and without SOC confirms localized *f*-electrons in a flat band near E_F , and the details of electronic bands without SOC are provided in Sec. VII of SI [27]. Our calculations, in the presence of SOC and the magnetic spin aligned along [001], show that crossing points appear along Γ -X and Γ -M due to the interaction between Nd *f*-orbitals and Ga *p*-orbitals, as shown in Fig. 3a. While the *f*-bands remain largely flat, they exhibit weak dispersion near these crossings, forming non-trivial nodal points. We have also calculated the Berry curvature along the same k-path, which further confirms the non-trivial nature of the identified nodal points, as shown in Sec. VII of SI [27].

The inclusion of localized *f*-electrons as occupied states can significantly impact the BC and, consequently, lead to a large AHC in NdGaSi. It is noteworthy that NdAlSi, in which the localized states lie well above the E_F , does not exhibit any measurable AHC [13, 20]. Fig. 3b represents the field-dependent Hall resistivity (ρ_{yx}) curve measured with $I \parallel [010]$ and $B \parallel [001]$ at various temperatures. At 30 K ($> T_C$), ρ_{yx} is linear with increasing magnetic field, as expected for a metallic system with carrier concentration (n) $\sim 9.2 \times 10^{22}$ cm⁻³. Below T_C , the anomalous Hall resistivity (ρ_{yx}^A) becomes prominent above a minuscule magnetic field of ~ 0.3 T and exhibits a linear trend up to 9 T, mimicking the magnetization isotherms [27]. Conventionally, the total Hall resistivity in a FM can be represented as $\rho_{yx}(B) = \rho_{yx}^O + \rho_{yx}^A = R_0 B + R_s \mu_0 M$, where ρ_{yx}^O and ρ_{yx}^A are the ordinary and anomalous contributions to the total Hall resistivity, with R_0 and R_s being the ordinary and anomalous Hall coefficients, respectively [43–45].

The Hall conductivity (σ_{xy}) is determined from the tensor relation $\sigma_{xy} = \rho_{yx}/(\rho_{xx}^2 + \rho_{yx}^2)$ as a function of the magnetic field [27]. Using zero-field extrapolation of high-field σ_{xy} data on the *y*-axis, we have extracted the AHC, denoted by σ_{xy}^A . Remarkably, $\sigma_{xy}^A \sim 1730 \Omega^{-1}$ cm⁻¹ at 2 K, with a subtle change up to 8 K in the ordered regime (Fig. 3c), among the largest in 4*f*-electron systems and comparable to the largest known itinerant

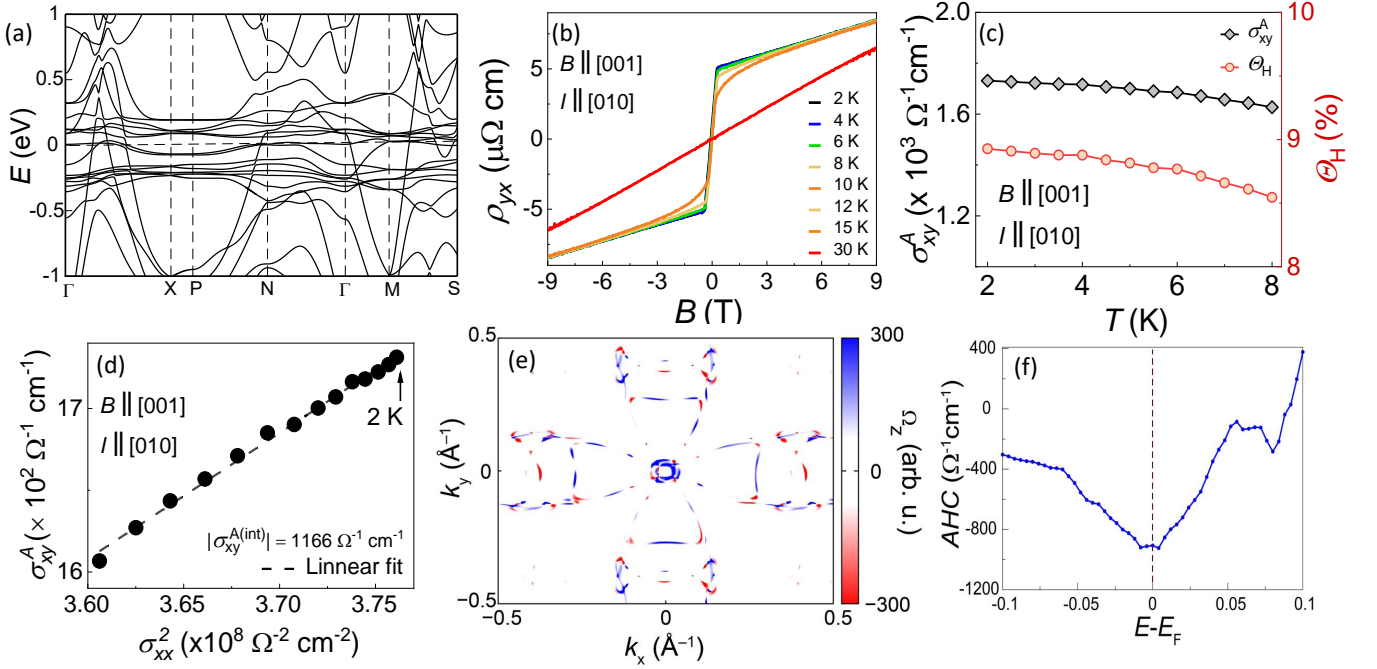


FIG. 3. (a) The band structure of NdGaSi with SOC in the FM state with the spins aligned along [001]. (b) Magnetic field-dependent Hall resistivity (ρ_{yx}) at different temperatures ranging from 2 K to 30 K with $B \parallel [001]$ and $I \parallel [010]$. (c) Temperature dependence of the anomalous Hall conductivity (σ_{xy}^A) and anomalous Hall angle (Θ_H). (d) Linear fitting of anomalous Hall conductivity σ_{xy}^A vs. σ_{xx}^2 curve. (e) BC distribution of NdGaSi in the first Brillouin zone reveals regions of maximum positive and negative values, depicted in red and blue, respectively. (f) Energy-dependent AHC obtained from the first-principles calculations.

3d systems to the best of our knowledge [2–4, 8, 46–48]. We have noticed a large anomalous Hall angle (AHA) of $\sim 9.3\%$ at 2 K (Fig. 3c).

AHE in NdGaSi occurs at very low temperatures (< 11 K), nullifying the role of phonon scattering and suggesting domination by residual resistivity (ρ_{xx0}). In such a scenario, σ_{xy}^A can be scaled using the empirical formula $\sigma_{xy}^A = (\alpha\sigma_{xx0}^{-1} + \beta\sigma_{xx0}^{-2})\sigma_{xx}^2 + m$, where σ_{xx0} is the residual longitudinal conductivity and the coefficients α , β , and m correspond to the skew-scattering, side jump, and the intrinsic Berry phase contributions to σ_{xy}^A , respectively [49, 50]. The m (or $\sigma_{xy}^{A,int}$) is determined by employing a linear fitting between σ_{xy}^A and σ_{xx}^2 as plotted in Fig. 3d. The $\sigma_{xy}^{A,int}$, thus, obtained is equal to $1166 \Omega^{-1} \text{cm}^{-1}$, further suggesting that the intrinsic Berry phase mechanism dominates the AHE in NdGaSi, however, the contribution of the scattering-dependent terms cannot be ignored. If one considers that each Nd layer independently contributes a quantum conductance of e^2/h , then the total BC-related AHC can be estimated to be $e^2/hd \sim 1080 \Omega^{-1} \text{cm}^{-1}$, where e is the electronic charge, h is the Planck constant, and d is the inter-layer spacing between two consecutive Nd layers [51]. This is quite close to our estimation of $\sigma_{xy}^{A,int} = 1166 \Omega^{-1} \text{cm}^{-1}$ from the scaling analysis. Finally, to confirm the reproducibility, we have measured σ_{xy}^A at 2 K with $B \parallel [001]$ and $I \parallel$

[010] for several NdGaSi single crystals, as described in Sec. VIII D of SI [27].

The large intrinsic AHC in experiments must arise from the BC associated with non-trivial crossings in the electronic band structure below E_F . $\sigma_{xy}^{A,int}$ can be calculated using the Kubo formalism within the framework of linear response theory [52] and it is written as function of z -component of BC (Ω_z), with further details provided in Sec VII of SI [27]. Ω_z is shown in the k_x - k_y plane for $k_z = 0$ in first Brillouin zone (see Fig. 3e). Fig. 3f presents the energy-dependent AHC, highlighting a significant contribution near E_F . Our calculations predict an AHC magnitude of $934 \Omega^{-1} \text{cm}^{-1}$, which is in excellent agreement with our experimental measurements for the material. Small carrier doping, i.e, small change in E_F , shows a weak effect on the AHC as evident from Fig. 3f.

We observe a complex interplay between magnetism that arises from localized f -electrons and topology in the electronic band structure in NdGaSi. The enhanced Sommerfeld coefficient and the Kadowaki-Woods ratio underscore moderate electron correlations and enhanced carrier localization of conduction electrons due to the presence of flat bands at E_F . Band structure calculations reveal quasi-flat $4f$ -bands of Nd at E_F , in agreement with our experimental observations. Consequently, a substantial BC arises from emerging Weyl points generated by

the crossing of the f -bands with dispersive bands. This corroborates the experimentally observed giant intrinsic AHC. We propose that the manipulation of the magnetic ground state provides a straightforward yet powerful tool to fully exploit the flat bands. By finely tuning the magnetic interactions to achieve just a sufficient magnitude of band splitting, one can relocate the localized states at E_F and harness their exotic properties. Our work provides a robust framework for utilizing localized f -bands to control large AHE in rare-earth intermetallic compounds and pave a pathway for engineering the band structure in real materials, enabling the exploration of these otherwise elusive states.

ACKNOWLEDGEMENTS

NK acknowledges DST for financial support through Grant Sanction No. CRG/2021/002747 and Max Planck Society for funding under the Max Planck-India partner group project. This research project made use of the instrumentation facility provided by the Technical Research Centre (TRC) at the S.N. Bose National Centre for Basic Sciences, under the Department of Science and Technology, Government of India. JS and MK acknowledge National Supercomputing Mission (NSM) for providing computing resources of ‘PARAM RUDRA’ at S.N. Bose National Centre for Basic Sciences, which is implemented by C-DAC and supported by the Ministry of Electronics and Information Technology (MeitY) and Department of Science and Technology (DST), Government of India.

* manoranjan.kumar@bose.res.in

† nitesh.kumar@bose.res.in

- [1] B. Johansson, Energy position of $4f$ levels in rare-earth metals, *Physical Review B* **20**, 1315 (1979).
- [2] E. Liu, Y. Sun, N. Kumar, L. Muechler, A. Sun, L. Jiao, S.-Y. Yang, D. Liu, A. Liang, Q. Xu, *et al.*, Giant anomalous Hall effect in a ferromagnetic kagome-lattice semimetal, *Nature Physics* **14**, 1125 (2018).
- [3] A. K. Nayak, J. E. Fischer, Y. Sun, B. Yan, J. Karel, A. C. Komarek, C. Shekhar, N. Kumar, W. Schnelle, J. Kübler, *et al.*, Large anomalous Hall effect driven by a nonvanishing Berry curvature in the noncolinear antiferromagnet Mn_3Ge , *Science Advances* **2**, e1501870 (2016).
- [4] S. Nakatsuji, N. Kiyohara, and T. Higo, Large anomalous Hall effect in a non-collinear antiferromagnet at room temperature, *Nature* **527**, 212 (2015).
- [5] S. N. Guin, Q. Xu, N. Kumar, H.-H. Kung, S. Dufresne, C. Le, P. Vir, M. Michiardi, T. Pedersen, S. Gorovikov, *et al.*, 2D-Berry-curvature-driven large anomalous hall effect in layered topological nodal-line $MnAlGe$, *Advanced Materials* **33**, 2006301 (2021).
- [6] H.-Y. Yang, B. Singh, J. Gaudet, B. Lu, C.-Y. Huang, W.-C. Chiu, S.-M. Huang, B. Wang, F. Bahrami, B. Xu, *et al.*, Noncollinear ferromagnetic Weyl semimetal with anisotropic anomalous Hall effect, *Physical Review B* **103**, 115143 (2021).
- [7] M. S. Alam, A. Fakhredine, M. Ahmad, P. Tanwar, H.-Y. Yang, F. Tafti, G. Cuono, R. Islam, B. Singh, A. Lynnyk, *et al.*, Sign change of anomalous Hall effect and anomalous Nernst effect in the Weyl semimetal $CeAlSi$, *Physical Review B* **107**, 085102 (2023).
- [8] C. Shekhar, N. Kumar, V. Grinenko, S. Singh, R. Sarkar, H. Luetkens, S.-C. Wu, Y. Zhang, A. C. Komarek, E. Kampert, *et al.*, Anomalous Hall effect in Weyl semimetal half-Heusler compounds $RPtBi$ ($R = Gd$ and Nd), *Proceedings of the National Academy of Sciences* **115**, 9140 (2018).
- [9] C. Dhital, R. L. Dally, R. Ruvalcaba, R. Gonzalez-Hernandez, J. Guerrero-Sanchez, H. B. Cao, Q. Zhang, W. Tian, T. Wu, M. D. Frontzek, S. K. Karna, A. Meads, B. Wilson, R. Chapai, D. Graf, J. Bacsá, R. Jin, and J. F. DiTusa, Multi- k magnetic structure and large anomalous Hall effect in candidate magnetic Weyl semimetal $NdAlGe$, *Physical Review B* **107**, 224414 (2023).
- [10] Y. Zhou, K.-H. Jin, H. Huang, Z. Wang, and F. Liu, Weyl points created by a three-dimensional flat band, *Physical Review B* **99**, 201105 (2019).
- [11] W. Jiang, D. J. De Sousa, J.-P. Wang, and T. Low, Giant anomalous Hall effect due to double-degenerate quasiflat bands, *Physical Review Letters* **126**, 106601 (2021).
- [12] M. Wang, W. Jiang, and Y. Yao, Three-dimensional flat band evolution between pyrochlore and perovskite lattices with enhanced anomalous Hall effect, *Physical Review B* **109**, 165147 (2024).
- [13] J. Gaudet, H.-Y. Yang, S. Baidya, B. Lu, G. Xu, Y. Zhao, J. A. Rodriguez-Rivera, C. M. Hoffmann, D. E. Graf, D. H. Torchinsky, *et al.*, Weyl-mediated helical magnetism in $NdAlSi$, *Nature Materials* **20**, 1650 (2021).
- [14] G. Chang, B. Singh, S.-Y. Xu, G. Bian, S.-M. Huang, C.-H. Hsu, I. Belopolski, N. Alidoust, D. S. Sanchez, H. Zheng, *et al.*, Magnetic and noncentrosymmetric Weyl fermion semimetals in the $RAlGe$ family of compounds ($R =$ rare earth), *Physical Review B* **97**, 041104 (2018).
- [15] T. Suzuki, L. Savary, J.-P. Liu, J. W. Lynn, L. Balents, and J. G. Checkelsky, Singular angular magnetoresistance in a magnetic nodal semimetal, *Science* **365**, 377 (2019).
- [16] P. Puphal, V. Pomjakushin, N. Kanazawa, V. Ukleev, D. J. Gawryluk, J. Ma, M. Naamneh, N. C. Plumb, L. Keller, R. Cubitt, *et al.*, Topological magnetic phase in the candidate Weyl semimetal $CeAlGe$, *Physical Review Letters* **124**, 017202 (2020).
- [17] M. Lyu, J. Xiang, Z. Mi, H. Zhao, Z. Wang, E. Liu, G. Chen, Z. Ren, G. Li, and P. Sun, Nonsaturating magnetoresistance, anomalous Hall effect, and magnetic quantum oscillations in the ferromagnetic semimetal $PrAlSi$, *Physical Review B* **102**, 085143 (2020).
- [18] X. Yao, J. Gaudet, R. Verma, D. E. Graf, H.-Y. Yang, F. Bahrami, R. Zhang, A. A. Aczel, S. Subedi, D. H. Torchinsky, *et al.*, Large topological Hall effect and spiral magnetic order in the Weyl semimetal $SmAlSi$, *Physical Review X* **13**, 011035 (2023).
- [19] R. Yamada, T. Nomoto, A. Miyake, T. Terakawa, A. Kikkawa, R. Arita, M. Tokunaga, Y. Taguchi, Y. Tokura, and M. Hirschberger, Nernst effect of high-

- mobility Weyl electrons in NdAlSi enhanced by a Fermi surface nesting instability, *Physical Review X* **14**, 021012 (2024).
- [20] J.-F. Wang, Q.-X. Dong, Z.-P. Guo, M. Lv, Y.-F. Huang, J.-S. Xiang, Z.-A. Ren, Z.-J. Wang, P.-J. Sun, G. Li, *et al.*, NdAlSi: A magnetic Weyl semimetal candidate with rich magnetic phases and atypical transport properties, *Physical Review B* **105**, 144435 (2022).
- [21] J.-F. Wang, Q.-X. Dong, Y.-F. Huang, Z.-S. Wang, Z.-P. Guo, Z.-J. Wang, Z.-A. Ren, G. Li, P.-J. Sun, X. Dai, *et al.*, Quantum oscillations in the magnetic Weyl semimetal NdAlSi arising from strong Weyl fermion- $4f$ electron exchange interaction, *Physical Review B* **108**, 024423 (2023).
- [22] M. Piva, J. Souza, G. Lombardi, K. Pakuszewski, C. Adriano, P. Pagliuso, and M. Nicklas, Topological Hall effect in CeAlGe, *Physical Review Materials* **7**, 074204 (2023).
- [23] D. Ram, S. Malick, Z. Hossain, and D. Kaczorowski, Magnetic, thermodynamic, and magnetotransport properties of CeGaGe and PrGaGe single crystals, *Physical Review B* **108**, 024428 (2023).
- [24] J. Gong, H. Wang, K. Han, X.-Y. Zeng, X.-P. Ma, Y.-T. Wang, J.-F. Lin, X.-Y. Wang, and T.-L. Xia, Anomalous Hall effect in an antiferromagnetic CeGaSi single crystal, *Physical Review B* **109**, 024434 (2024).
- [25] L.-B. Zhang, Q.-X. Dong, J.-L. Bai, Q.-Y. Liu, J.-W. Cheng, C.-D. Li, P.-Y. Liu, Y.-R. Sun, Y. Huang, Z.-A. Ren, *et al.*, Magnetism, heat capacity, magnetocaloric effect, and magneto-transport properties of heavy fermion antiferromagnet CeGaSi, *Chinese Physics B* **33**, 067101 (2024).
- [26] J. Bouaziz, G. Bihlmayer, C. E. Patrick, J. Staunton, and S. Blügel, Origin of incommensurate magnetic order in the RAlSi (R = Pr, Nd, Sm) magnetic Weyl semimetals, *Physical Review B* **109** (2024).
- [27] See the Supplementary Information for the details of sample characterization and additional supporting data.
- [28] J. Železný, H. Gao, A. Manchon, F. Freimuth, Y. Mokrousov, J. Zemen, J. Mašek, J. Sinova, and T. Jungwirth, Spin-orbit torques in locally and globally noncentrosymmetric crystals: Antiferromagnets and ferromagnets, *Physical Review B* **95**, 014403 (2017).
- [29] N. Mott and H. Jones, *The theory of the properties of metals and alloys*, Oxf. Univ. Press, London (1936).
- [30] D. Kaczorowski and A. Szytuła, Magnetic, thermal and electrical transport properties of TmAuGe, *Journal of Alloys and Compounds* **614**, 186 (2014).
- [31] D. Ram, L. Joshi, and Z. Hossain, Crystalline electric field and large anomalous Hall effect in NdGaGe single crystals, *Journal of Magnetism and Magnetic Materials* **605**, 172326 (2024).
- [32] U. Walter, Treating crystal field parameters in lower than cubic symmetries, *Journal of Physics and Chemistry of Solids* **45**, 401 (1984).
- [33] E. Gopal, *Specific heats at low temperatures* (Springer Science & Business Media, 2012).
- [34] J. Campoy, E. Plaza, A. Coelho, and S. Gama, Magnetoresistivity as a probe to the field-induced change of magnetic entropy in RAl₂ compounds (R = Pr, Nd, Tb, Dy, Ho, Er), *Physical Review B—Condensed Matter and Materials Physics* **74**, 134410 (2006).
- [35] A. Szytuła, D. Kaczorowski, K. Nenkov, *et al.*, Electronic structure and magnetism of RPdIn compounds (R = La, Ce, Pr, Nd), *Solid State Communications* **142**, 556 (2007).
- [36] G. Grimvall, The electron-phonon interaction in normal metals, *Physica Scripta* **14**, 63 (1976).
- [37] Y. Xiao, Y. Chen, H. Ni, Y. Li, Z. Wen, Y. Cui, Y. Zhang, S. Liu, C. Wang, R. Zhong, *et al.*, Preparation, crystal structure, and properties of the kagome metal ThV₆Sn₆, *Inorganic Chemistry* **63**, 23288 (2024).
- [38] H. Maletta, V. Sechovsky, P. Veenhuizen, F. De Boer, L. Havela, and G. Hilscher, From itinerant antiferromagnetism towards localized ferromagnetism in UNi (Al, Ga), *Zeitschrift für Physik B Condensed Matter* **72**, 455 (1988).
- [39] A. Andreev, Y. Homma, Y. Shiokawa, and V. Sechovský, Magnetic properties of the UC₀Al_{1-x}Ga_x intermetallic system, *Journal of Alloys and Compounds* **269**, 34 (1998).
- [40] K. Kadowaki and S. Woods, Universal relationship of the resistivity and specific heat in heavy-fermion compounds, *Solid State Communications* **58**, 507 (1986).
- [41] M. Rice, Electron-electron scattering in transition metals, *Physical Review Letters* **20**, 1439 (1968).
- [42] A. Jacko, J. Fjærestad, and B. Powell, A unified explanation of the Kadowaki–Woods ratio in strongly correlated metals, *Nature Physics* **5**, 422 (2009).
- [43] N. Nagaosa, J. Sinova, S. Onoda, A. H. MacDonald, and N. P. Ong, Anomalous Hall effect, *Reviews of Modern Physics* **82**, 1539 (2010).
- [44] R. Karplus and J. Luttinger, Hall effect in ferromagnetics, *Physical Review* **95**, 1154 (1954).
- [45] T. Jungwirth, Q. Niu, and A. MacDonald, Anomalous Hall effect in ferromagnetic semiconductors, *Physical Review Letters* **88**, 207208 (2002).
- [46] Y. Arai, J. Hayashi, K. Takeda, H. Tou, H. Sugawara, and H. Kotegawa, Intrinsic anomalous Hall effect arising from antiferromagnetism as revealed by high-quality NbMnP, *Journal of the Physical Society of Japan* **93**, 063702 (2024).
- [47] B. Meng, H. Wu, Y. Qiu, C. Wang, Y. Liu, Z. Xia, S. Yuan, H. Chang, and Z. Tian, Large anomalous Hall effect in ferromagnetic Weyl semimetal candidate PrAlGe, *APL Materials* **7** (2019).
- [48] Y. Wang, C. Xian, J. Wang, B. Liu, L. Ling, L. Zhang, L. Cao, Z. Qu, and Y. Xiong, Anisotropic anomalous Hall effect in triangular itinerant ferromagnet Fe₃GeTe₂, *Physical Review B* **96**, 134428 (2017).
- [49] Y. Tian, L. Ye, and X. Jin, Proper scaling of the anomalous Hall effect, *Physical Review Letters* **103**, 087206 (2009).
- [50] D. Hou, G. Su, Y. Tian, X. Jin, S. A. Yang, and Q. Niu, Multivariable scaling for the anomalous Hall effect, *Physical Review Letters* **114**, 217203 (2015).
- [51] D. Xiao, M.-C. Chang, and Q. Niu, Berry phase effects on electronic properties, *Reviews of modern physics* **82**, 1959 (2010).
- [52] M. Gradhand, D. Fedorov, F. Pientka, P. Zahn, I. Mertig, and B. Györffy, First-principle calculations of the Berry curvature of Bloch states for charge and spin transport of electrons, *Journal of Physics: Condensed Matter* **24**, 213202 (2012).